HYDROLOGICAL PROCESSES
Hydrol. Process. (2016)
Published online in Wiley Online Library
(wileyonlinelibrary.com) DOI: 10.1002/hyp.10869

Impact of climate indicators on continental-scale potential groundwater recharge in Africa

Paolo Nasta,[1]* John B. Gates[1] and Yoshihide Wada[2,3,4,5]

[1] *Department of Earth and Atmospheric Sciences, University of Nebraska, Lincoln, NE, USA*
[2] *NASA Goddard Institute for Space Studies, 2880 Broadway, New York, NY, 10025, USA*
[3] *Center for Climate Systems Research, Columbia University, 2880 Broadway, New York, NY, 10025, USA*
[4] *Department of Physical Geography, Faculty of Geosciences, Utrecht University, Heidelberglaan2, 3584, CS, Utrecht, The Netherlands*
[5] *International Institute for Applied Systems Analysis, Schlossplatz 1, A-2361, Laxenburg, Austria*

Abstract:

In the last decades, human activity has been contributing to climate change that is closely associated with an increase in temperatures, increase in evaporation, intensification of extreme dry and wet rainfall events, and widespread melting of snow and ice. Understanding the intricate linkage between climate warming and the hydrological cycle is crucial for sustainable management of groundwater resources, especially in a vulnerable continent like Africa. This study investigates the relationship between climate-change drivers and potential groundwater recharge (PGR) patterns across Africa for a long-term record (1960–2010). Water-balance components were simulated by using the PCR-GLOBWB model and were reproduced in both gridded maps and latitudinal trends that vary in space with minima on the Tropics and maxima around the Equator. Statistical correlations between temperature, storm occurrences, drought, and PGR were examined in six climatic regions of Africa. Surprisingly, different effects of climate-change controls on PGR were detected as a function of latitude in the last three decades (1980–2010). Temporal trends observed in the Northern Hemisphere of Africa reveal that the increase in temperature is significantly correlated to the decline of PGR, especially in the Northern Equatorial Africa. The climate indicators considered in this study were unable to explain the alarming negative trend of PGR observed in the Sahelian region, even though the Standardized Precipitation-Evapotranspiration Index (SPEI) values report a 15% drought stress. On the other hand, increases in temperature have not been detected in the Southern Hemisphere of Africa, where increasing frequency of storm occurrences determine a rise of PGR, particularly in southern Africa. Time analysis highlights a strong seasonality effect, while PGR is in-phase with rainfall patterns in the summer (Northern Hemisphere) and winter (Southern Hemisphere) and out-of-phase during the fall season. This study helps to elucidate the mechanism of the processes influencing groundwater resources in six climatic zones of Africa, even though modelling results need to be validated more extensively with direct measurements in future studies.

KEY WORDS potential groundwater recharge; rainfall; drought; seasonality; storm frequency; Africa

Received 12 October 2015; Accepted 30 March 2016

INTRODUCTION

Groundwater is an essential natural resource for urban, industrial, and agricultural water supply and socioeconomic development (de Vries and Simmers, 2002). It has been projected that rapid population growth will force a significant increase in freshwater demands in many regions of the world (Wada *et al*., 2011). The degree to which groundwater resources can sustain increased abstraction is highly uncertain, given the current scarcity of groundwater recharge estimates (Döll *et al*., 2014; McLaughlin and KinzelBach, 2015). Climate-change impacts on renewable freshwater resources add another layer of uncertainty with regard to future pressures on water availability, accessibility, and demand.

Understanding how climate drives the spatiotemporal distribution of groundwater recharge rates triggered below the vadose zone has been explored in existing studies in different areas of the world (Eckhardt and Ulbrich, 2003; Brouyere *et al*., 2004; Keese *et al*., 2005; Ng *et al*., 2010; Green *et al*., 2011; Kim and Jackson, 2011; Crosbie *et al*., 2013; Panwar and Chakrapani, 2013; Faramarzi *et al*., 2013). Rainfall can be considered as the major climatic driver in affecting recharge rates, with particular emphasis on rainfall intensity and frequency distribution. Studies related to climate change suggest that a greater increase in extreme precipitation will exacerbate the frequency of heavy rainfall events in some regions and increase the risk of more prolonged drought spells in other regions (Milly *et al*., 2005). Regional-scale studies

*Correspondence to: Paolo Nasta, Department of Earth and Atmospheric Sciences, University of Nebraska-Lincoln, 211 Bessey Hall, Lincoln, NE 68588, USA.
E-mail: paolo.nasta@unina.it

in North America provide evidence of a decreasing trend in groundwater recharge under (historical or projected) global warming (Rosenberg *et al.*, 1999; Ferguson and George, 2003). Other important climatic factors include solar radiation and vapor deficit, which significantly impact groundwater recharge rates in tropical zones (Vivoni *et al.*, 2009; Barron *et al.*, 2012).

Groundwater is a crucial resource in Africa, where the population at risk of increased water stress is projected to be over 500 million people by 2050 (Burke *et al.*, 2009; Carter and Parker, 2009; MacDonald *et al.*, 2012). A sustainable and efficient water management carefully regulates withdrawals such that water is not overused when rainfall is not able to replenish the groundwater stocks. Thus, there is an urgent necessity to examine the sensitivity of groundwater recharge to climate-change indicators in Africa (MacDonald *et al.*, 2009). The challenge is to assist regional policy makers in Africa in acquiring more knowledge on vulnerable groundwater resources by capturing recharge response to extreme climate impacts (Shongwe *et al.*, 2009; Shongwe *et al.*, 2011).

Field studies of groundwater recharge in Africa have had uneven spatial coverage (Edmunds, 2009; Bonsor and MacDonald, 2010). As a result, there is currently a pressing need for large-scale recharge estimates to underpin sustainable water-resource management strategies (Döll and Fiedler, 2008; Nyenje and Batelaan, 2009). In order to fill the information gap, this study addresses spatiotemporal variability in continental-scale groundwater recharge rates using a global hydrologic model (PCR-GLOBWB) with daily boundary forcings and a high spatial resolution. We note that the model has not been calibrated for Africa; hence, this investigation *de facto* represents a large-scale sensitivity analysis. The term 'potential groundwater recharge' is therefore used to refer only to a synthetic model approximation of direct measurements in Africa. The results have been validated by few available direct-recharge measurements retrieved in the scientific literature. The main objectives of this study are twofold: (1) assessing the impact of climate-change drivers on spatial distribution and spatiotemporal trends of average annual PGR in Africa; and (2) analysing inter-annual and seasonal variability of PGR. This novel contribution provides valuable insights in detecting the historical relationships between climate-change indicators and groundwater recharge in Africa. The groundwater recharge rates simulated with a continental-scale bucket model represent, to date, the primary data used to assess the influence of climatic controls on unconfined aquifers in Africa. Therefore the observed trends in six climatic regions in Africa can be used to develop analogs for groundwater recharge responses that can be exploited in scenario-based approaches under future climate-change projections.

METHODOLOGY

PCR-GLOBWB model

The PCR-GLOBWB (PCRaster-GLOBal Water Balance) is a grid-based bucket model of global terrestrial hydrology (van Beek *et al.*, 2011; Wada *et al.*, 2014; http://pcraster.geo.uu.nl/). For each grid cell (spatial resolution of $0.1° \times 0.1°$), this model simulates the water exchange between the atmosphere and two vertically stacked soil layers connected to a third underlying groundwater layer. The PCR-GLOBWB model refers to the units of meter (m) and day (d) for the dimensions of length (L) and time (T), respectively. Rainfall ($L\,T^{-1}$) and snowmelt ($L\,T^{-1}$) represent the inflow to the hydrologic system. Runoff ($L\,T^{-1}$) and evaporation ($L\,T^{-1}$) contribute to water loss from the soil surface. Vegetation affects the water balance through transpiration ($L\,T^{-1}$) and canopy interception ($L\,T^{-1}$). The soil hydraulic parameters are assigned according to eleven soil-texture classes corresponding to different soil types based on the FAO Digital Soil Map of the World (FAO, 2003).

Groundwater recharge (downward flux) and capillary rise (upward flux) represent the vertical water exchanges between the second and third subsurface soil layers (Wada *et al.*, 2010). Downward water fluxes (percolation and groundwater recharge) among the three soil layers are calculated using the unit-gradient form of the Darcy–Buckingham equation. Groundwater recharge interacts with groundwater storage through capillary rise if the top of the groundwater level is within ~5 m of the topographical surface (Wada *et al.*, 2012; Wada *et al.*, 2014). Groundwater storage is fed by groundwater recharge and drained as baseflow by a reservoir coefficient that includes information on lithology and topography (e.g. hydraulic conductivity of the subsoil; maps can be visualized in http://www.bgs.ac.uk/research/groundwater/international/africangroundwater/maps.html).

The ensuing capillary rise is calculated as the upward moisture flux that can be sustained when an upward gradient exists and the moisture content of the soil is below field capacity. Additionally, the capillary rise cannot exceed the available storage in the underlying groundwater reservoir.

The model was forced with daily fields of precipitation, reference (potential) evapotranspiration, and temperature for the 1960–2010 period. For the 1960–1978 period, boundary forcings were prescribed by the ERA40 re-analysis data. The associated climate data are publicly available at http://www.ecmwf.int/en/forecasts/datasets/era-40-dataset-sep-1957-aug-2002. In order to extend our analysis to the year 2010, we forced the model by comparable daily climate fields taken from the ERA-Interim re-analysis data, from which we obtained daily fields

of temperature, reference potential evapotranspiration, and GPCP-corrected precipitation (GPCP: Global Precipitation Climatology Project; http://www.gewex.org/gpcp.html). For compatibility with our overall analysis, the ERA40 data analysis was bias-corrected on a grid-by-grid basis by scaling the long-term monthly means of the daily climate fields (precipitation, evapotranspiration, and temperature) to those of the ERA-Interim data for the overlapping reference climate for 1979–2001. We then further bias-corrected the modified climate dataset by scaling the long-term monthly means of the daily climate fields to those from the Climate Research Units (CRU) TS 2.1 time-series (Mitchell and Jones, 2005), wherever station coverage by the CRU is adequate for the overlapping period. The associated climate data are publicly available at http://www.cru.uea.ac.uk/data. For the ERA40 re-analysis data, we separately bias-corrected for the 1960s and 1970s period to correct the overestimation of precipitation present over the tropics during the 1970s (Hempel *et al*., 2013; Wada *et al*., 2014; Wada and Bierkens, 2014).

Model limitations

We caution that the continental-scale lumped-parameter approach provides only a crude approximation of the water budget and is possible at the cost of several simplifications: (1) ignoring preferential flow into the soil, fractured rock, saprolite (Neuman, 2005; Beven and Germann, 2013), and karst regions (Hartmann *et al*., 2015); (2) not considering the role of macroporosity (Owor *et al*., 2009; Taylor *et al*., 2013); (3) missing proper soil-hydraulic properties pertaining to datasets related to specific Tropical and Equatorial zones in Africa (Minasny and Hartemink, 2011); (4) missing information on land-use changes (urbanization, deforestation) in Africa (Githui *et al*., 2009; Baker and Miller, 2013); (5) lacking records of water pumping and the role of human consumption of water; and (6) ignoring focused recharge via leakage from surface waters (ephemeral streams, wetlands, or lakes). Therefore, we caution that the model might not be able to simulate actual recharge rates in some regions and, for this reason, we will refer only to 'potential groundwater recharge' (PGR) in the remainder of the manuscript (Rushton, 1997).

In order to test the above limitations of the model, we compiled 13 published groundwater recharge rates (Table I) obtained primarily by field techniques, namely chloride mass balance (CMB), water table fluctuations (WTF), groundwater residence time (GRT) with the use of tracers, and water balance (WB) (BredenKamp *et al*., 1995; Scanlon *et al*., 2002; Wang *et al*., 2010). The spatial resolution (SP), mean (μ) values, and ranges of average annual observed groundwater recharge rates are reported with the corresponding simulated values in PCR-GLOBWB (Table I).

The Nash–Sutcliffe Efficiency (NSE%) index has been calculated for the analysis of agreement between observed (GR_{obs}) and simulated (GR_{sim}) groundwater recharge (GR):

Table I. List of bibliographic references in 13 countries of Africa reporting spatial resolution (SP), average (μ), range (min and max), and method of measured recharge. PCR-GLOBWB simulated recharge values are reported as well and compared to measured recharge rates through the relative differences (RD)

	Observations						Simulations	
Country	Reference	SP km^2	μ $m\,yr^{-1}$	min $m\,yr^{-1}$	max $m\,yr^{-1}$	method	PCR-GLOBWB $m\,yr^{-1}$	RD %
Botswana	de Vries *et al*. (2000) †	4875	0.005	0.001	0.010	CMB	0.003	7.1
Burundi	Bakundukize *et al*. (2011)	1050	0.235	0.141	0.306	WB	0.345	−26.6
Cameroon	Fouépé Takounjou *et al*. (2011)	11	0.108	0.016	0.237	WTF + CMB	0.252	−38.1
Ethiopia	Demlie *et al*. (2007)	1500	0.265	0.088	0.418	GRT	0.189	25.4
Niger	Leduc *et al*. (1997)	595	0.055	0.050	0.060	WTF + CMB	0.005	84.6
Nigeria	Edmunds (2009) †	18 000	0.030	0.014	0.049	CMB	0.088	−30.8
Senegal	Edmunds (2009) †	1600	0.016	0.005	0.034	CMB	0.069	−35.4
Sudan	Abdalla (2009) †	60 000	0.006	0.004	0.008	GRT	0.036	−35.1
Tanzania	Nkotagu (1996) †	—	0.013	0.010	0.016	CMB	0.075	−40.4
Togo	Akouvi *et al*. (2008)	3500	0.063	0.038	0.088	GRT	0.139	−28.7
Uganda	Taylor *et al*. (2013) †	840	0.200	—	—	WB	0.294	−23.9
Zambia	Houston (1982) †	40	0.080	—	—	WB	0.118	−15.4
Zimbabwe	Sibanda *et al*. (2009)	—	0.025	0.002	0.062	WTF + CMB + GRT	0.049	−18.0

† Included in Bonsor and MacDonald (2010).

$$\mathrm{NSE}\% = \left[1 - \frac{\sum_{i=1}^{N}\left(GR_{obs,i} - GR_{sim,i}\right)^2}{\sum_{i=1}^{N}\left(GR_{obs,i} - \overline{GR_{obs}}\right)^2}\right] \times 100 \quad (1)$$

where N is the number of recharge observations ($N = 13$), and $\overline{GR_{obs}}$ is the arithmetic mean of observed groundwater recharge. High values of NSE% (near 100%) indicate best agreements, whereas a value of 50% (i.e. NSE% > 50%) can be assumed as a threshold for efficient and acceptable agreements (Moriasi *et al.*, 2007). Near-zero or negative values of NSE% ($0 > \mathrm{NSE}\% > -\infty$) indicate unacceptable performances provided by the model simulations (Bennett *et al.*, 2013).

Despite the fact that the NSE% = 30.6% is below the threshold of satisfactory efficiency (NSE% < 50%), the performance can be considered sufficiently acceptable, considering that the model was not calibrated. The relative differences (RD), expressed in percentages of the $\log_{10}$-values listed in the right-hand column of Table I, indicate that most of the modelled recharge rates tend to overestimate the measurements. The best model performances are observed in countries in southern Africa (Botswana, Zambia, and Zimbabwe), albeit preferential flow plays an important role in controlling recharge rates measured with chloride mass balance (de Vries *et al.*, 2000). Higher discrepancies are reported in countries of Sahelian Africa (Niger, Sudan).

DATA PROCESSING

The set of input and output data in Africa for the 51-year time period (1960–2010) was taken from the existing database of worldwide simulations executed by the PCR-GLOBWB model (Wada *et al.*, 2014). Gridded parameter values, boundary forcings, and simulation results were mapped using ArcMap 10.1. Statistical analyses were completed in a parallel computing environment that adapted MATLAB into a super-computing cluster (http://hcc.unl.edu/tusker/index.php). The scripts can be made available upon request.

The analysis of extreme-rainfall variability considered two statistical indicators describing storm occurrences (f_{max}) and mean dry consecutive days (τ_{dry}) (Small, 2005). The former expresses the number of storms (all those values above the annual mean value) over the total number of rainfall events, while the latter is identified through the mean dry interval time between two separate rainfall events.

Average annual values of boundary forcings, namely rainfall (P) and potential evapotranspiration ($\mathrm{ET_p}$), are displayed in Figure 1, whereas simulated water-balance components, namely potential groundwater recharge (PGR), actual evapotranspiration ($\mathrm{ET_a}$), and runoff ($\mathrm{Q_r}$), are shown in Figure 2.

The continental-scale spatial distribution of average annual PGR and $\mathrm{Q_r}$ broadly follows the precipitation distribution (Goddard and Graham, 1999; Sultan and Janicot, 2000).

The African continent has a heterogeneous distribution of renewable freshwater resources. Water availability is mostly concentrated in the humid zones around the Equator. The remaining areas experience permanent arid conditions with modest or insignificant recharge generation (Schuol *et al.*, 2008). Nevertheless, the humid areas are characterized by a high degree of spatial and temporal variability of groundwater recharge rates. On a latitudinal-averaged basis, the mean annual PGR reaches maxima near the Equator ($0.42\,\mathrm{m\,yr^{-1}}$ at latitude -0.45°N) and minima near the tropics ($0.00028\,\mathrm{m\,yr^{-1}}$ at 20.05°N and $0.012\,\mathrm{m\,yr^{-1}}$ at -25.35°N, respectively) (Figure 2).

The Mann–Kendall nonparametric test (Mann, 1945; Kendall, 1975) has been calculated in order to detect eventual temporal trends in long-time series for annual temperature (T), rainfall indicators (f_{max},τ_{dry}), and PGR. The Mann–Kendall test is expressed by:

$$S = \sum_{i=1}^{N-1}\sum_{j=i+1}^{N} sgn\left(x_j - x_i\right) \quad (2)$$

where x_i and x_j are the sequential data values, N (the total number of years is 51 between 1960 and 2010) is the length of data series, and *sgn* is the sign function. For a large number of years, S is assumed to be normally distributed with an expected value E(S) = 0 and

$$\mathrm{var}(S) = \frac{N(N-1)(2N+5)}{18}. \quad (3)$$

The standardized test statistic Z_c is calculated as:

$$Z_c = \begin{cases} (S-1)/\mathrm{var}(S)^{1/2} & S > 0 \\ 0 & S = 0 \\ (S+1)/\mathrm{var}(S)^{1/2} & S < 0 \end{cases}. \quad (4)$$

The null hypothesis indicating no trend is accepted when $|Z_c| \le Z_{1-\alpha/2}$, where α is the significance level, and $Z_{1-\alpha/2}$ is the standard normal quantile at probability level of $1-\alpha/2$. Therefore, the trend test is based on the following two conditions:

(1) $Z_c < -Z_{1-\alpha/2}$ indicates decreasing trend; and
(2) $Z_c > Z_{1-\alpha/2}$ indicates increasing trend.

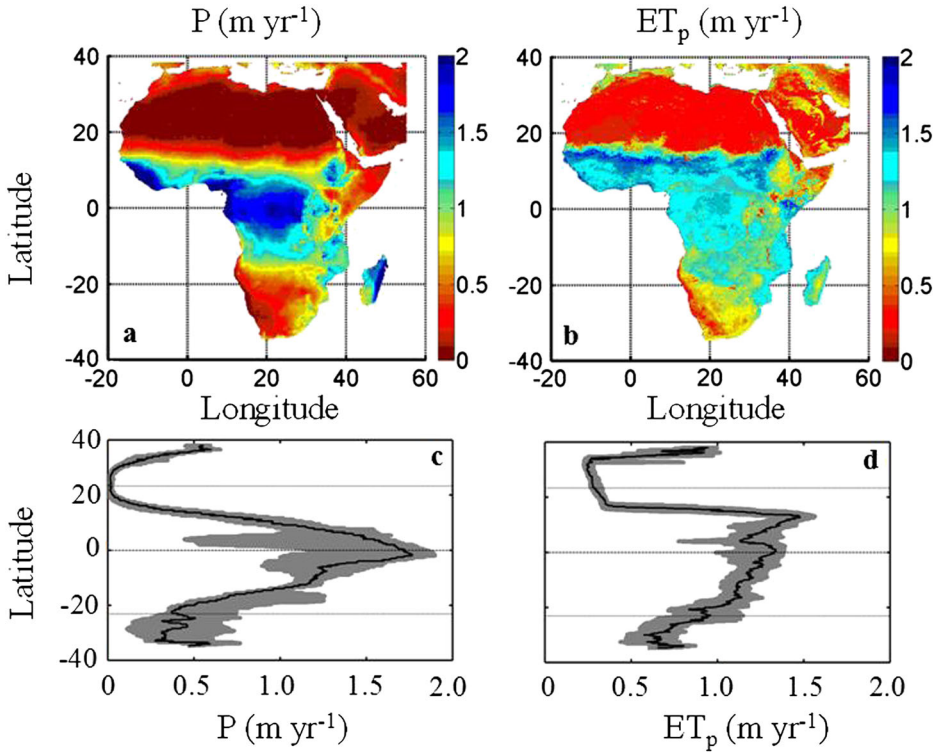

Figure 1. Gridded maps of average annual (a) rainfall (P) and (b) potential evapotranspiration (ET_p); latitudinal patterns of average annual (c) P and (d) ET_p. The ranges of values between the 25th and 75th percentiles are represented by the gray bands. The horizontal dotted lines represent the Tropic of Cancer and the Tropic of Capricorn, while the horizontal dashed line depicts the Equator

In this study, we fixed α at the 0.05 significance level, and $Z_{1-\alpha/2} = 1.96$.

RESULTS AND DISCUSSIONS

Spatial distribution of PGR

The objective of this subsection is to characterize PGR spatial patterns in Africa and to identify statistical relationships between average annual rainfall and PGR on a latitudinal-averaged basis. Trambauer *et al.* (2014) recently defined six climatic regions, namely Mediterranean (MED), Sahel (SAH), North Equatorial Central Africa (NEQ), Horn of Africa (HORN), South Equatorial Central Africa (SEQ), and Southern Africa (SAFR). These six regions were based on the existing map of five climate classes (hyper-arid, arid, semi-arid, dry sub-humid, and humid) according to the aridity index, defined as the ratio between mean-annual rainfall and mean-annual evaporation (Figure3a).

PGR occurs significantly only in the North (21% area) and South (12% area) Equatorial Central Africa (NEQ + HORN and SEQ) regions with $0.27\,m\,yr^{-1}$ and $0.26\,m\,yr^{-1}$, respectively (Figure 3b). PGR is lower than $0.05\,m\,yr^{-1}$ in the remaining four regions (MED, SAH, HORN, and SAFR) that cover the major part of Africa. In addition to climate drivers, biophysical controls, such as geomorphology, soil stratigraphy, lithology, and land use, play a paramount role in determining the spatial variability of the water-balance components (Beauvais, 1999; Farmer *et al.*, 2003; Kim and Jackson, 2011). Longitudinal variabilities of PGR, ET_a, and Q_r increase with rainfall along the Equatorial latitudes, as designated by the larger gray-shaded areas depicted in Figure 2d–f.

The highest rates of PGR are observed in the NEQ and SEQ regions (0.29 and $0.26\,m\,yr^{-1}$, respectively) (Table II). The coefficients of variation (CV) values are relatively low (12% and 15%, respectively). The recharge rate in the Mediterranean region is one order of magnitude lower than that of central Africa ($0.0215\,m\,yr^{-1}$), whereas the remaining three regions have recharge rates of two orders of magnitude lower than those in Equatorial Africa with the highest degree of spatial variability (CV > 100%). Average recharge rates of $0.05\,m\,yr^{-1}$ as simulated in the PCR-GLOBWB model in the SAH region support previous measurements in chloride profiles that range between 0.03 and $0.15\,m\,yr^{-1}$ (Scanlon *et al.*, 2006).

The latitudinal relationships between average annual rainfall and PGR in each climatic region (HORN is combined with NEQ) demonstrate that all correlation coefficients (R^2) are significantly high ($0.75 < R^2 < 0.88$), implying that PGR is highly dependent on average annual

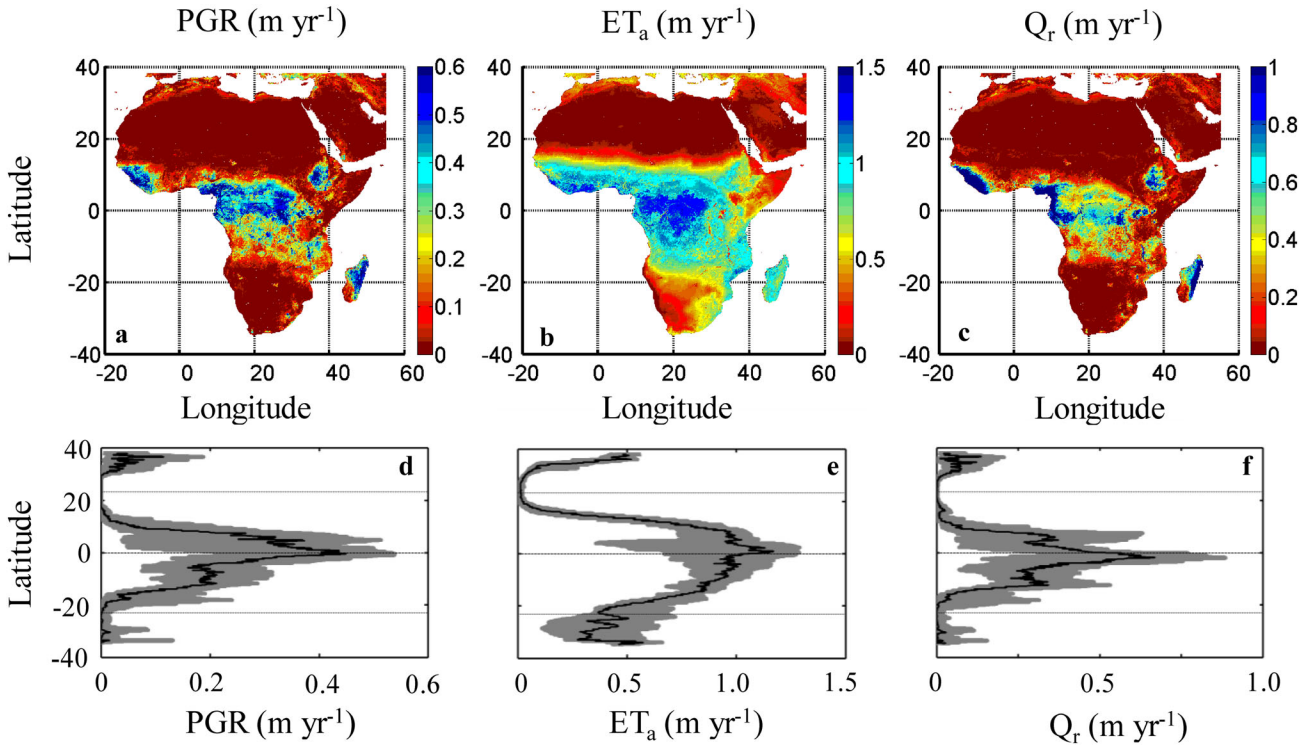

Figure 2. Gridded maps of average annual (a) potential groundwater recharge (PGR), (b) actual evapotranspiration (ET_a), and (c) runoff (Q_r); latitudinal patterns of average annual (d) PGR, (e) ET_a, and (f) Q_r. The ranges of values between the 25th and 75th percentiles are represented by the gray bands. The horizontal dotted lines represent the Tropic of Cancer and the Tropic of Capricorn, while the horizontal dashed line depicts the Equator

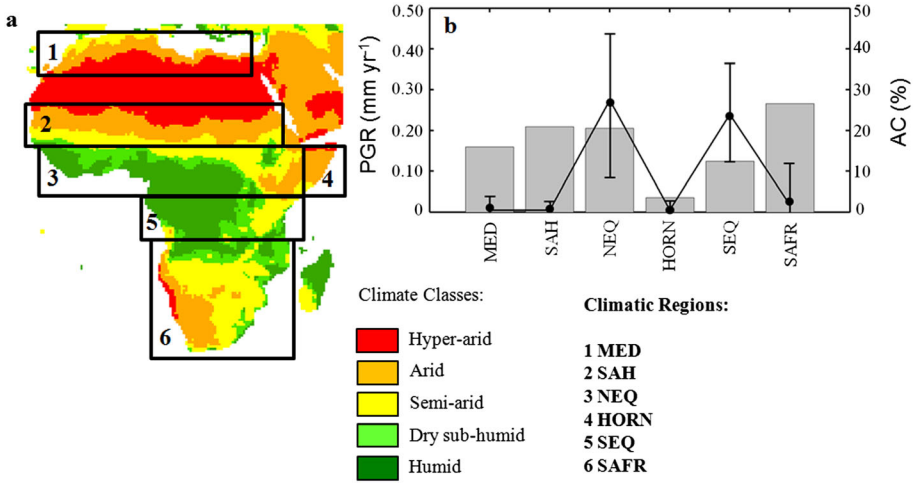

Figure 3. (a) Gridded patterns of the five climate classes and six climatic regions in Africa; (b) average annual PGR (black circles) delimited by the 25th and 75th percentiles in each climatic region (vertical black lines). The gray bar charts depict the relative contributing areas, AC (%)

rainfall patterns (Figure 4). We observe that the lowest correlation value ($R^2 = 0.75$) in the MED region is significantly affected by a strong drying latitudinal (north–south) gradient. The northern semi-arid half portion ($37° < \text{lat} < 32°$) of the MED region is characterized by high spatial variability and very low correlation between P and PGR. Conversely, in the southern hyper-arid half portion outside of the mountainous headwaters ($32° < \text{lat} < 27°$) of the MED region, P and PGR are reduced by three times but exhibited high correlation. The regression line grade (indicated by the slope-values) gets steeper in Central Africa (NEQ + HORN and SEQ) and three times lower in the other three climatic zones (MED, SAH, and SAFR), where the average annual rate of PGR

Table II. Descriptive statistics of precipitation (P) and potential groundwater recharge (PGR) with mean (μ), standard deviation (σ), coefficient of variation (CV), minimum (min), and maximum (max) in the six climatic regions of Africa (MED, SAH, NEQ + HORN, SEQ, and SAFR)

		MED $27° < \text{lat} < 37°$		SAH $10° < \text{lat} < 20°$		NEQ + HORN $0° < \text{lat} < 10°$		SEQ $-10° < \text{lat} < 0°$		SAFR $-35° < \text{lat} < -10°$	
		P	PGR	P	PGR	P	PGR	P	PGR	P	PGR
μ	$m\,yr^{-1}$	0.22	0.04	0.40	0.05	1.24	0.27	1.32	0.26	0.68	0.08
σ	$m\,yr^{-1}$	0.17	0.03	0.31	0.05	0.12	0.06	0.12	0.07	0.27	0.07
CV	%	79	80	80	118	9	22	9	27	40	82
min	$m\,yr^{-1}$	0.02	0	0.03	0	0.99	0.14	1.18	0.18	0.36	0
max	$m\,yr^{-1}$	0.60	0.12	0.94	0.15	1.48	0.38	1.52	0.42	1.19	0.24

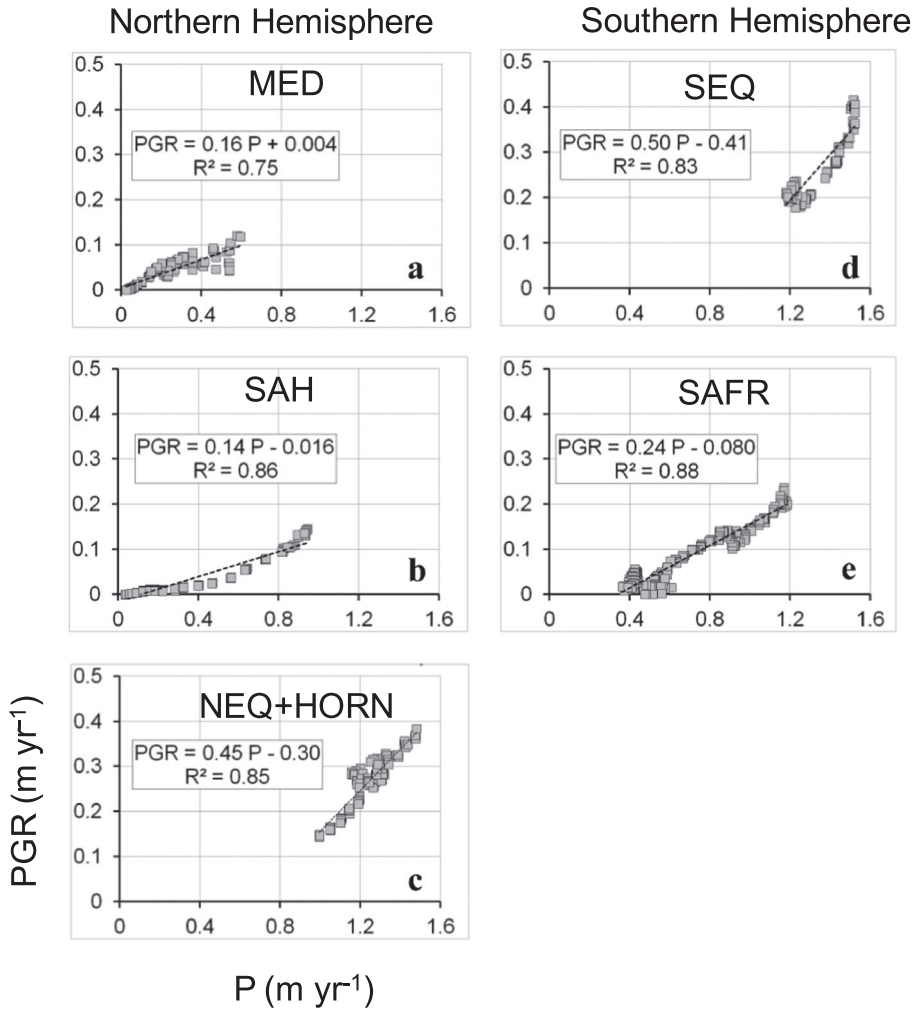

Figure 4. Relationship between average annual rainfall (P) and potential groundwater recharge (PGR) values (gray squares) along with trend lines (dotted lines) and correlation coefficients (R^2) in (a) MED, (b) SAH, (c) NEQ + HORN, (d) SEQ, and (e) SAFR

is only between 14% and 24% of P on a latitudinal-averaged basis.

The spatial distribution of climate-indicators, namely storm occurrences and drought, reflects different patterns in the two Hemispheres (Figure 5).

The extreme rainfall parameter, f_{max}, increases between the Equator and the Tropic of Capricorn, with the peak at −12.95°N ($f_{max} = 0.42$), meaning that about 40% of rainfall events have intensities higher than their mean values. The values of τ_{dry} emphasize the importance of

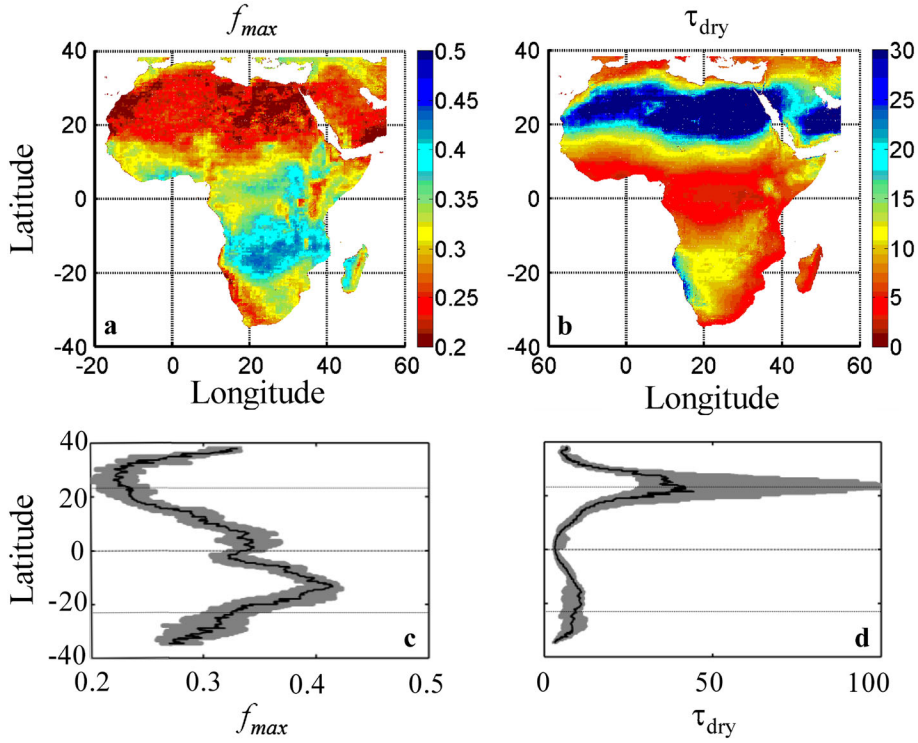

Figure 5. Gridded maps of (a) storm occurrences (f_{max}) and (b) mean dry consecutive days (τ_{dry}); latitudinal patterns of (c) f_{max} and (d) τ_{dry}. The ranges of values between the 25th and 75th percentiles are represented by the gray bands. The horizontal dotted lines represent the Tropic of Cancer and the Tropic of Capricorn, while the horizontal dashed line depicts the Equator

episodic rainfall events in the hyper-arid areas of the Northern Hemisphere and follow a similar trend along the latitude with a cusped shape in proximity to the Tropic of Cancer characterized by a high degree of longitudinal variability. A modest increase of τ_{dry} is detected above the Tropic of Capricorn.

Temporal variability of PGR

Inter-annual variability of PGR. This section addresses the empirical understanding of how climate-change drivers have been related to PGR in the last three decades (1980–2010).

The Spearman's correlation coefficients between PGR and climate-change indicators (temperature and the two extreme rainfall distribution indicators; see Table III) highlight a general negative correlation between temperature (T) and PGR, with zero effect on the MED, SAH, and HORN regions, with a modest impact on SEQ (−0.20), and with a significant influence on NEQ (−0.48) and SAFR (−0.76) (Tashie *et al.*, 2015). While the relationship between rainfall and temperature is difficult to characterize, the correlation between potential evapotranspiration (ET_p) and temperature is often positive (Kingston and Taylor, 2010).

The parameter, f_{max}, has a very low impact in the arid regions of Africa, with the exception of SAFR, whereas significant correlation is observed in Equatorial Africa. The increase in storm occurrences favours both PGR and Q_r generation in humid Equatorial regions of Africa. Indeed, in the model setup, the former is driven by gravity and is greatest under saturated conditions, while the latter occurs under the same circumstances but when rainfall exceeds soil-infiltration capacity. The parameter τ_{dry} significantly affects the two extreme regions (MED and SAFR) with correlations values of −0.45 and −0.38, respectively, while the impacts in the humid regions are relatively low.

The Mann–Kendall test results pertaining to the last three decades of model simulations (1980–2010) elucidate the temporal evolution of climate indicators and PGR (Table IV). The temperature exhibits increasing trends in the MED, SAH, and NEQ zones, but not in the Southern

Table III. Spearman's correlation coefficients between PGR and temperature (T) and rainfall indicators (f_{max}, τ_{dry}) in the six climatic regions of Africa (MED, SAH, NEQ, HORN, SEQ, and SAFR)

	MED	SAH	NEQ	HORN	SEQ	SAFR
T	−0.10	−0.09	−0.48	0.03	−0.20	−0.76
τ_{dry}	−0.45	−0.19	−0.01	−0.12	−0.06	−0.38
f_{max}	0.03	−0.01	0.45	0.06	0.39	0.59

Table IV. Mann–Kendall trend test for annual temperature (T), rainfall indicators (f_{max}, τ_{dry}), and potential groundwater recharge (PGR) in the six climatic regions of Africa (MED, SAH, NEQ, HORN, SEQ, and SAFR). Significant positive and negative values are indicated in bold text

	MED	SAH	NEQ	HORN	SEQ	SAFR
T	**4.59**	**3.94**	**3.54**	0.56	0.78	−0.68
τ_{dry}	−0.08	−0.85	−1.17	−0.10	−0.22	−0.12
f_{max}	−0.14	−1.82	1.53	0.75	−1.02	**3.55**
PGR	−0.03	**−2.07**	**−2.58**	1.84	−0.27	**2.33**

Hemisphere of Africa. The extreme rainfall indicators also signal an increasing trend of f_{max} in SAFR (Min *et al*., 2011). Nevertheless, PGR shows decreasing trends in SAH and NEQ and an increasing trend in SAFR. In view of the significant trends reported in Table IV and considering the correlation coefficients listed in Table III, we can infer that climate change is significantly impacting PGR only in the SAH, NEQ, and SAFR climatic zones. The two zones above the Equator indicate negative correlation between temperature and PGR, whereas the latter shows a high positive correlation value between f_{max} and PGR.

It is interesting to note that temperature is increasing only in the Northern Hemisphere of Africa. This implies a general decrease in PGR in the zones above the Equator, in contrast to a general temporal stability of climatic-change drivers and hydrological balance in the Southern Hemisphere. The climate-temporal variation in each climatic zone has been objectively analysed through the Standardized Precipitation–Evapotranspiration Index (SPEI) (Vicente-Serrano *et al*., 2010) downloaded from the website http://sac.csic.es/spei/database.html (Beguería *et al*., 2014). This multi-scalar drought index has the advantage of combining the effect of precipitation and potential evapotranspiration demand (affected by temperature) and is particularly valuable for the application of future projections (Lorenzo-Lacruz *et al*., 2010). For the purpose of showing an illustrative example, a transect along longitude 15.25°E has been identified by considering latitudes 28.25°N, 15.25°N, 5.25°N, −5.25°N, and −22.25°N for the MED, SAH, NEQ, SEQ, and SAFR zones, respectively. Very dry conditions characterized by negative SPEI values are observed in the 1930s, 1940s, and 1970s in the MED zone, the 1970s, 1980s, and 1990s in the SAH zone, the 1930s in the NEQ zone, the 1950s in the SEQ zone, and the 1920s, 1980s, and 1990s in the SAFR zone (Figure 6). This qualitative visual inspection confirms the high-climatic variability among the different zones of Africa. However, we considered the temporal SPEI values in all cells pertaining to each climatic zone. Thus, it is possible to compare the frequency distribution of the SPEI values in the time range (1901–2010) with the distribution belonging to the last three decades of model simulations (1980–2010) in order to identify the causes of the trends observed in Table IV. The frequency distributions of SPEI values (blue bars) in the entire range with an expected SPEI mean around zero approximately partition 50% of wet and 50% of dry conditions (Figure 7). The frequency distributions of SPEI values (red bars) pertaining to the last three decades in the Northern Hemisphere of Africa are affected by a shift to the left by lowering the probabilities of observing wet conditions by 4.4%, 14.8%, and 6% for MED, SAH, and NEQ, respectively. Decreasing trend of PGR is observed in the SAH and NEQ zones, but not in the MED region (Table IV). The devastating drought spells in the SAH zone in the last three decades probably represent the most prevalent climatic changes in Africa that have significantly decreased PGR. On the other hand, the two zones (SEQ and SAFR) in the Southern Hemisphere report a slight increase in wet conditions in the last three decades, increasing by 1.5% and 1% in the SEQ and SAFR zones, respectively. The climatic stability observed in the SEQ zone impedes any trend for PGR, although the climate and PGR statistics of NEQ and SEQ (observed in Tables I, II, and III; Figure 4) are very similar. Based on

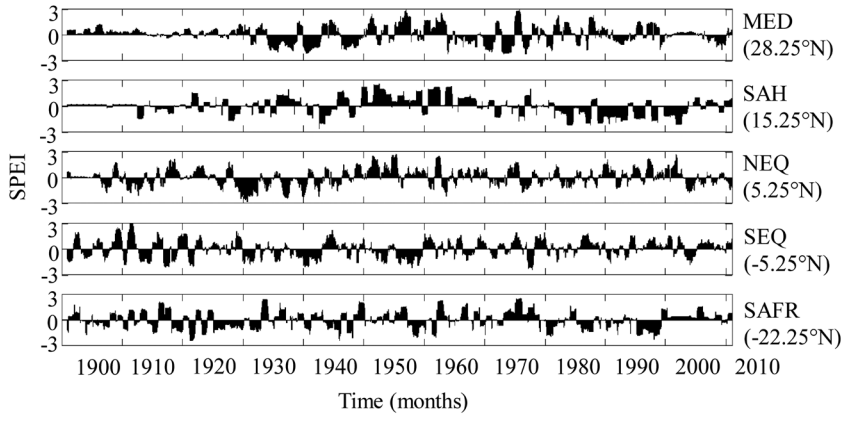

Figure 6. Temporal evolution of 12-month SPEI values from 1901 to 2013 along the transect at longitude 15.25°E

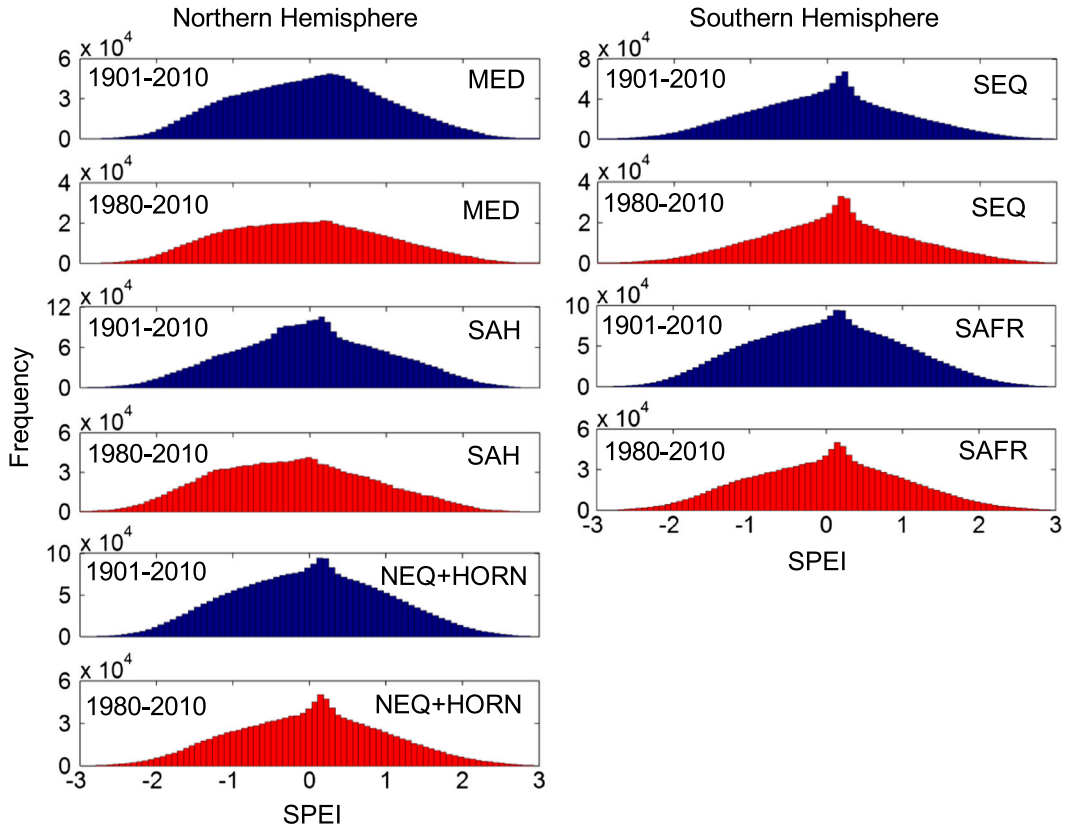

Figure 7. Frequency distribution of the 12-month SPEI values from 1901 to 2010 (blue bars) and from 1980 to 2010 (red bars) in the six climatic regions of Africa (MED, SAH, NEQ + HORN, SEQ, and SAFR)

the historic data, our findings support the future projections described by Faramarzi *et al*. (2013) that predict an increase up to 400% of blue water in Southern Africa (albeit small) and a decrease of renewable water resources by 25–100% in the semi- and hyper-arid regions of Africa that will become more susceptible to severe drought conditions. Döll and Flörke (2005) evaluated the impact of climate change on long-term, average annual diffuse groundwater recharge, as simulated by the global hydrological WaterGAP Global Hydrology Model. By applying four different climate-change scenarios between the present day and the 2050s, they have predicted a significant increase in groundwater recharge by up to 30% in the SAH and HORN regions, while decreasing trends are expected in the MED and southwestern SAFR regions.

Site-specific studies in Africa support our findings. Ruelland *et al*. (2012) predict a decrease of rainfall by 15–17% and a rise in potential evapotranspiration by 16–18% in the Bani River catchment located in Mali (SAH region), resulting in a critical reduction of water availability. The effects of climate change on groundwater recharge in the upper Ssezibwa catchment, Uganda (the SEQ region) have been investigated by Nyenje and Batelaan (2009), who implemented a hydrological model for simulating future climate-change scenarios. They predict a combined increase of rainfall and groundwater recharge by 100% in 2080.

Seasonality of PGR. The rainfall regimes during the four seasons are complex in both the Northern and Southern Hemispheres (Nicholson, 2000). Seasonal variation of P and PGR is considered both in gridded maps (Figure 8) and in latitudinal averaged basis (Figure 9). Seasonal rainfall maxima are observed in the SAH zone in summer and in the SAFR zone in winter. Nevertheless the Equatorial zones (NEQ and SEQ) are characterized by two rainy seasons (spring and fall). However, large longitudinal variability is observed in the MED and SAFR zones in winter.

In general, PGR is in-phase with rainfall patterns in the summer and winter, while the two regimes are out-of-phase in the Southern Hemisphere during the spring and in the Northern Hemisphere in the fall.

In the MED region (above the Tropic of Cancer), rainfall is mostly concentrated in the spring, fall, and winter. Episodic and intense rainfall events without PGR response occur in spring, especially over the Atlas Mountain range in northwestern Africa (Jasechko *et al*., 2014). The summer in this region is very dry, whereas fall

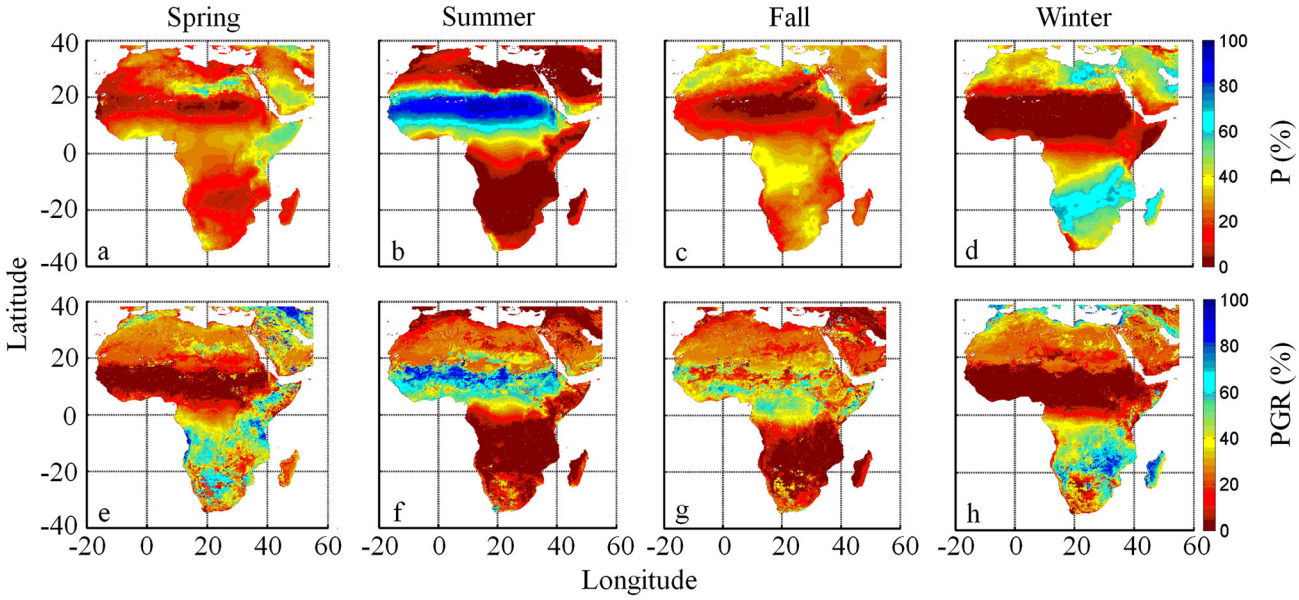

Figure 8. Gridded maps of P (top panel) and PGR (bottom panel) in spring, summer, fall, and winter

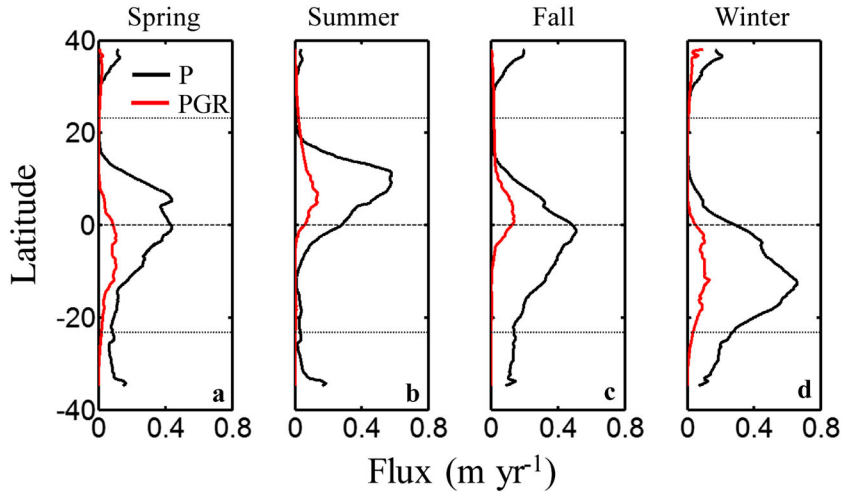

Figure 9. Latitudinal trends of P (black lines) and PGR (red lines) in spring, summer, fall, and winter. The horizontal dotted lines represent the Tropic of Cancer and the Tropic of Capricorn, while the horizontal dashed line depicts the Equator

and winter are characterized by rainfall events with recharge occurring only in winter (peak of 0.1 m yr^{-1} in the northern extreme). The winter is affected by a significant frequency of intense storms (high f_{max}-values; see Figure 5h) that trigger PGR occurrences in the vadose zone.

The region delimited by the two Tropics (which includes the southern portion of Sahel, Equatorial central Africa, Horn of Africa, and the northern portion of southern Africa) is affected by marked seasonal trends of rainfall and PGR. It is interesting to note that P and PGR oscillate with a moving bell-shaped curve, with minima corresponding to the two tropical lines and the maximum point over the Equator in spring and fall.

In the spring, P is almost symmetrically partitioned by the Equatorial line which delimits the maximum point (0.44 m yr^{-1}); conversely, PGR is 70% in the Southern Hemisphere and 30% in the Northern Hemisphere, with maxima (about 0.44 m yr^{-1}) spanning from the Equator down to the border between SEQ and SAFR. The rainfall over the Tropic of Capricorn is 0.08 m yr^{-1}. In the summer, the rainfall line shifts towards the north (79% rainfall in the north), with its peak at 11.05°N (about 0.60 m yr^{-1}), followed by PGR

Table V. Seasonal partition of P and PGR (in %) between Northern and Southern Hemispheres

	Spring		Summer		Fall		Winter	
	P %	PGR %	P %	PGR %	P %	PGR %	P %	PGR %
Northern Hemisphere	46	29	79	91	34	76	14	18
Southern Hemisphere	54	71	21	9	66	24	86	82

(91% recharge in the north), with its peak ($0.13\,m\,yr^{-1}$) at 7.35°N. In the fall, the rainfall line moves back and reaches its peak ($0.51\,m\,yr^{-1}$) immediately below the Equator (Table V). Surprisingly, we observed a rainfall value of $0.14\,m\,yr^{-1}$ in the Tropic of Capricorn, indicating a rainfall concentration over the area that includes Zimbabwe, Mozambique, and Botswana. Indeed, rainfall in this season is not symmetrically subdivided by the Equator, but with a disproportion of 66% in the Southern Hemisphere (mostly in the South Equatorial central Africa; Figure 9c) and 34% in the Northern Hemisphere. On the contrary, PGR remains concentrated in the Northern Hemisphere (76%) with its peak ($0.14\,m\,yr^{-1}$) above the Equator and a gradual decrease northward with zero values registered in central Sahel. Finally, in the winter, the rainfall line moves southward with its maximum point ($0.66\,m\,yr^{-1}$) at −11.25°N and 86% of rainfall in the Southern Hemisphere. The severe rainfall events prompt PGR, even in zones that remain arid for the rest of the year. In this period, the PGR follows the rainfall with a very similar proportion (82% in the south) and its peak of $0.13\,m\,yr^{-1}$ at −11.75°N.

CONCLUSIONS

Groundwater levels of shallow aquifers worldwide have been experiencing a decreasing trend over the last few decades. This is generally due to groundwater pumping surpassing groundwater recharge rates (Wada *et al*., 2014). Nonetheless, climate-related changes in groundwater recharges merit further analysis because their impact might alleviate or exacerbate the observed general decreasing trend (Loaiciga *et al*., 2000).

In light of future climate-change predictions, we are particularly interested in understanding how PGR reacts to temperature increases and changing storm characteristics, particularly because their impact on groundwater recharge remains poorly understood in Africa. The conditions that favour or limit PGR over evapotranspiration or runoff generation depend largely on the nonlinear unsaturated zone response to rainfall. These results highlight the three main following potential consequences in climate-change conditions caused by continental warming: (1) increasing temperatures occurring in the Northern Hemisphere can potentially trigger a decrease of PGR, especially in the NEQ region; (2) the decreasing trend of PGR observed in the last three decades in the SAH region is not correlated to the temperature or τ_{dry}, even though the SPEI values point out a notable decrease of 15% of probability for wet conditions; and (3) storm occurrences affect the humid regions of Equatorial Africa (NEQ and SEQ), and the increasing trends of f_{max} and PGR have been observed in SAFR for the last 30 years. Therefore, the rise in temperature and storm occurrences, which can be considered warning signs of climate change, impact PGR in contrasting modes in the Northern and Southern Hemispheres of Africa. These outcomes align with previous continental-scale predictions carried out by Faramarzi *et al*. (2013), and the observed historical trends partially contrast future projections provided by Döll and Flörke (2005).

Temporal analysis reveals the role of seasonality with evident latitudinal patterns and disproportional distribution of rain and PGR between the Northern and Southern Hemispheres. The rainfall and PGR regimes are out of phase in the spring and fall, and synchronous in the summer and winter.

In view of the empirical relations observed in this study, future scenarios can concentrate on specific statistical analyses to link storm characteristics and temperature variations with PGR in simplistic models used for water-resources management. The observed model uncertainty is high all across Africa, with the exception of SAFR. Therefore, the outcomes observed in our analysis might be potentially realistic only for southern Africa. Nonetheless, we emphasize the importance of offering coarse guidelines on the relations between climate change and PGR as representing preliminary outcomes for future applications, that will be hopefully tested by direct groundwater-recharge measurements.

ACKNOWLEDGEMENTS

This project was supported by the 'Robert B. Daugherty Water for Food Institute—Nebraska Water Center at the University of Nebraska'. The authors wish to thank Ludovicus P. H. van Beek and Marc F. P. Bierkens for providing the access to the dataset of the PCR-GLOBWB model. We are grateful to Adam Caprez for helping to set up the data processing in the super-computing cluster. Y. Wada is supported by the Japan Society for the Promotion of Science (JSPS) Overseas Research Fellowship (grant no. JSPS-2014-878).

REFERENCES

Akouvi A, Dray M, Violette S, de Marsily G, Zuppi GM. 2008. The sedimentary coastal basin of Togo: example of a multilayered aquifer still influenced by a palaeo-seawater intrusion. *Hydrogeology Journal* **16**: 419–436.

Bakundukize C, van Camp M, Walraevens K. 2011. Estimation of groundwater recharge in Bugusera region (Burundi) using soil moisture budget approach. *Geologica Belgica* **14**: 85–102.

Baker TJ, Miller SN. 2013. Using the Soil and Water Assessment Tool (SWAT) to assess land use impact on water resources in an East African watershed. *Journal of Hydrology* **486**: 100–111.

Barron OV, Crosbie RS, Dawes WR, Charles SP, Pickett T, Donn MJ. 2012. Climatic controls on diffuse groundwater recharge across Australia. *Hydrology and Earth System Sciences* **16**. DOI:10.5194/hess-16-4557-2012.

Beauvais A. 1999. Geochemical balance of lateritization processes and climatic signatures in weathering profiles overlain by ferricretes in Central Africa. *Geochimica et Cosmochimica Acta* **63**: 3939–3957.

Beguería S, Vicente-Serrano SM, Reig F, Latorre B. 2014. Standardized precipitation evapotranspiration index (SPEI) revisited: parameter fitting, evapotranspiration models, tools, datasets and drought monitoring. *International Journal of Climatology*. DOI:10.1002/joc.3887.

Bennett ND, Croke BFW, Guariso G, Guillaume JHA, Hamilton SH, Jakeman AJ, Marsili-Libelli S, Newham LTH, Norton JP, Perrin C, Pierce SA, Robson B, Seppelt R, Voinov AA, Fath BD, Andreassian V. 2013. Characterising performance of environmental models. *Environmental Modelling and Software* **26**: 92–102.

Beven K, Germann P. 2013. Macropores and water flow in soils revisited. *Water Resources Research* **49**. DOI:10.1002/wrcr.20156.

Bonsor HC, MacDonald AM. 2010. Groundwater and climate change in Africa: review of recharge studies. British Geological Survey Internal Report, IR/10/075, 30 pp.

Bredenkamp DB, Botha LJ, VT Gj, Van Resburg JH. 1995. Manual on quantitative estimation of groundwater recharge and aquifer storativity. Water Research Commission Report TT73/95. Pretoria, South Africa.

Brouyere S, Carabin G, Dassargues A. 2004. Climate change impacts on groundwater resources: modelled deficits in a chalky aquifer, Geer basin, Belgium. *Hydrogeology Journal* **12**(2): 123–134.

Burke MB, Lobell DB, Guarino L. 2009. Shifts in African crop climates by 2050, and the implications for crop improvement and genetic resources conservation. *Global Environmental Changes* **19**: 317–325.

Carter RC, Parker A. 2009. Climate change, population trends and groundwater in Africa. *Hydrological Sciences Journal* **54**(4): 676–689.

Crosbie RS, Scanlon BR, Mpelasoka FS, Reedy RC, Gates JB, Zhang L. 2013. Potential climate change effects on groundwater recharge in the High Plains Aquifer, USA. *Water Resources Research* **49**. DOI:10.1002/wrcr.20292.

de Vries JJ, Selaolo ET, Beekman HE. 2000. Groundwater recharge in the Kalahari, with reference to paleo-hydrologic conditions. *Journal of Hydrology* **238**: 110–123.

de Vries JJ, Simmers I. 2002. Groundwater recharge: an overview of processes and challenges. *Hydrogeology Journal* **10**: 5–17.

Demlie M, Wohnlich S, Gizaw B, Stichler W. 2007. Groundwater recharge in the Akaki catchment, central Ethiopia: evidence from environmental isotopes ($\delta^{18}O$, $\delta^{2}H$, and ^{3}H) and chloride mass balance. *Hydrological Processes* **21**: 807–818.

Döll P, Flörke M. 2005. Global-scale estimation of diffuse groundwater recharge. Frankfurt Hydrology Paper 03, Institute of Physical Geography, Frankfurt University, Frankfurt.

Döll P, Fiedler K. 2008. Global-scale modeling of groundwater recharge. *Hydrology and Earth System Sciences* **12**: 863–885.

Döll P, Müller Schmied H, Schuh C, Portmann FT, Eicker A. 2014. Global-scale assessment of groundwater depletion and related groundwater abstractions: combining hydrological modeling with information from well observations and GRACE satellites. *Water Resources Research* **50**. DOI:10.1002/2014WR015595.

Eckhardt K, Ulbrich U. 2003. Potential impacts of climate change on groundwater recharge and streamflow in a central European low mountain range. *Journal of Hydrology* **284**(1–4): 244–252.

Edmunds WME. 2009. Palaeoclimate and groundwater evolution in Africa —implications for adaptation and management. *Hydrological Sciences Journal* **54**: 781–792.

Faramarzi M, Abbaspour KC, Vaghefi SA, Farzaneh MRA, Zehnder JB, Srinivasan R, Yang H. 2013. Modeling impacts of climate change on freshwater availability in Africa. *Journal of Hydrology* **480**: 85–101.

Farmer D, Sivapalan M, Jothityangkoon C. 2003. Climate, soil, and vegetation controls upon the variability of water balance in temperate and semiarid landscapes: downward approach to water balance analysis. *Water Resources Research* **39**(2): 1035. DOI:10.1029/2001WR000328, 2003.

Ferguson G, George SS. 2003. Historical and estimated ground water levels near Winnipeg, Canada and their sensitivity to climatic variability. *Journal of the American Water Resources Association* **39**: 1249–1259.

Food and Agriculture Organization (FAO). 2003. Digital Soil Map of the World, Version 3.6., FAO, Rome, Italy. Available at http://www.fao.org/nr/land/soils/digital-soil-map-of-the-world (Accessed March 12, 2013).

Fouépé Takounjou A, Ndam Ngoupayou JR, Riotte J, Takem GE, Mafany G, Maréchal JC, Ekodeck GE. 2011. Estimation of groundwater recharge of shallow aquifer on humid environment in Yaounde, Cameroon using hybrid water-fluctuation and hydrochemistry methods. *Environmental Earth Sciences.* **64**: 107–118.

Githui F, Mutua F, Bauwens W. 2009. Estimating the impacts of land-cover change on runoff using the soil and water assessment tool (SWAT): case study of Nzoia catchment, Kenya. *Hydrological Sciences Journal* **54**(5): 899–908.

Goddard L, Graham NE. 1999. Importance of the Indian Ocean for simulating rainfall anomalies over eastern and southern Africa. *Journal of Geophysical Research* **104**: 19099–19116.

Green TR, Taniguchi M, Kooi H, Gurdak JJ, Allen DM, Hiscock KM, Treidel H, Aureli A. 2011. Beneath the surface of global change: impacts of climate change on groundwater. *Journal of Hydrology* **405**: 532–560.

Hartmann A, Gleeson T, Rosolem R, Pianosi F, Wada Y, Wagener T. 2015. A large-scale simulation model to assess karstic groundwater recharge over Europe and the Mediterranean. *Geoscientific Model Development* **8**: 1729–1746.

Hempel S, Frieler K, Warszawski L, Schewe J, Piontek F. 2013. A trend-preserving bias correction—the ISI-MIP approach. *Earth Systems Dynamics* **4**: 219–236.

Jasechko S, Birks SJ, Gleeson T, Wada T, Fawcett PJ, Sharp ZD, McDonnell JJ, Welker JM. 2014. The pronounced seasonality of global groundwater recharge. *Water Resources Research* **50**: 8845–8867. DOI:10.1002/2014WR015809.

Kendall MG. 1975. *Rank correlation measures*. Charles Griffin: London.

Keese KE, Scanlon BR, Reedy RC. 2005. Assessing controls on diffuse groundwater recharge using unsaturated flow modeling. *Water Resources Research* **41** W06010. DOI:10.1029/2004WR003841.

Kim JH, Jackson RB. 2011. A global analysis of groundwater recharge for vegetation, climate, and soils. *Vadose Zone Journal*. DOI:10.2136/vzj2011.0021RA.

Kingston DG, Taylor RG. 2010. Sources of uncertainty in climate change impacts on river discharge and groundwater in a headwater catchment of the Upper Nile Basin, Uganda. Hydrol. *Hydrology and Earth System Sciences* **14**: 1297–1308.

Leduc C, Bromley J, Schroeter P. 1997. Water table fluctuation and recharge in semi-arid climate: some results of the HAPEX-Sahel hydrodynamic survey (Niger). *Journal of Hydrology* **189**: 123–138.

Loaiciga HA, Maidment DR, Valdes JB. 2000. Climate-change impacts in a regional karst aquifer, Texas, USA. *Journal of Hydrology* **227**: 173–194.

Lorenzo-Lacruz J, Vicente-Serrano SM, López-Moreno JI, Beguería S, García-Ruiz JM, Cuadrat JM. 2010. The impact of droughts and water management on various hydrological systems in the headwaters of the Tagus River (central Spain). *Journal of Hydrology* **386**: 13–26.

MacDonald AM, Bonsor HC, Dochartaigh BEO, Taylor RG. 2012. Quantitative maps of groundwater resources in Africa. *Environmental Research Letters* **7**: 1–7, 024009. DOI:10.1088/1748-9326/7/2/024009.

MacDonald AM, Calow RC, MacDonald DM, Darling GW, Dochartaigh BEO. 2009. What impact will climate change have on rural

groundwater supplies in Africa? *Hydrological Sciences Journal* **54**(4): 690–703.

Mann HB. 1945. Non-parametric tests against trend. *Econometrica* **13**: 245–259.

McLaughlin D, Kinzelbach W. 2015. Food security and sustainable resource management. *Water Resources Research* **51**: 4966–4985.

Milly PCD, Dunne KA, Vecchia AV. 2005. Global pattern of trends in streamflow and water availability in a changing climate. *Nature* **438** (17): 347–350.

Min S, Zhang X, Zwiers F, Hegerl G. 2011. Human contribution to more-intense precipitation extremes. *Nature* **470**(7334): 378–381.

Minasny B, Hartemink AE. 2011. Predicting soil properties in the tropics. *Earth-Science Reviews* **106**: 52–62.

Mitchell TD, Jones PD. 2005. An improved method of constructing a database of monthly climate observations and associated high-resolution grids. *International Journal of Climatology* **25**: 693–712. DOI:10.1002/joc.1181.

Moriasi DN, Arnold JG, Van Liew MW, Bingner RL, Harmel RD, Veith TL. 2007. Model evaluation guidelines for systematic quantification of accuracy in watershed simulations. *Transactions of the ASABE* **50**(3): 885–900.

Neuman SP. 2005. Trends, prospects and challenges in quantifying flow and transport through fractured rocks. *Hydrogeology Journal* **13**: 124–147.

Ng GHC, McLaughlin D, Entekhabi D, Scanlon BR. 2010. Probabilistic analysis of the effects of climate change on groundwater recharge. *Water Resources Research* **46**: 7502–7502.

Nicholson SE. 2000. The nature of rainfall variability over Africa on time scales of decades to millennia. *Global and Planetary Change* **26**: 137–158.

Nyenje PM, Batelaan O. 2009. Estimating the effects of climate change on groundwater recharge and baseflow in the upper Ssezibwa catchment, Uganda. *Hydrological Sciences Journal* **54**(4): 713–726. DOI:10.1623/hysj.54.4.713.

Owor M, Taylor RG, Tindimugaya C, Mwesigwa D. 2009. Rainfall intensity and groundwater recharge: evidence from the Upper Nile Basin. *Environmental Research Letters* **4**. DOI:10.1088/1748-9326/4/3/035009.

Panwar S, Chakrapani GJ. 2013. Climate change and its influence on groundwater resources. *Current Science* **105**: 37–46.

Rosenberg NJ, Epstein DJ, Wang D, Vail L, Srinivasan R, Arnold JG. 1999. Possible impacts of global warming on the hydrology of the Ogallala aquifer region. *Climatic Change* **42**: 677–692.

Ruelland D, Ardoin-Bardin S, Collet L, Roucou P. 2012. Simulating future trends in hydrological regime of a large Sudano-Sahelian catchment under climate change. *Journal of Hydrology* **424**: 207–216.

Rushton K. 1997. Recharge from permanent water bodies. In *Recharge of phreatic aquifers in (semi) arid areas*. AA Balkema: Rotterdam; 215–255.

Scanlon BR, Healy RW, Cook PG. 2002. Choosing appropriate techniques for quantifying groundwater recharge. *Hydrogeology Journal* **10**: 18–39.

Scanlon BR, Keese KE, Flint AL, Flint LE, Gaye CB, Edmunds VM, Simmers I. 2006. Global synthesis of groundwater recharge in semiarid and arid regions. *Hydrological Processes* **20**(15): 3335–3370.

Schuol J, Abbaspour KC, Srinivasan R, Yang H. 2008. Modelling blue and green water availability in Africa. *Water Resources Research* **44**: W07406. DOI:10.1029/2007WR006609.

Shongwe ME, van Oldenborgh GJ, van den Hurk BJJM, de Boer B, Coelho CAS, van Aalst MK. 2009. Projected changes in mean and extreme precipitation in Africa under global warming. Part I: southern Africa. *Journal of Climatology* **22**: 3819–3837.

Shongwe ME, van Oldenborgh GJ, van den Hurk BJJM, van Aalst MK. 2011. Projected changes in mean and extreme precipitation in Africa under global warming. Part II: east Africa. *Journal of Climatology* **24**: 3718–3733.

Sibanda T, Nonner J, Uhlenbrook S. 2009. Comparison of groundwater recharge estimation methods for the semi-arid Nyamandhlovu area, Zimbabwe. *Hydrogeology Journal* **17**: 1427–1441.

Small EE. 2005. Climatic controls on diffuse groundwater recharge in semiarid environments of the southwestern United States. *Water Resources Research* **41**: W04012. DOI:10.1029/2004WR003193.

Sultan B, Janicot S. 2000. Abrupt shift of the ITCZ over West Africa and intra-seasonal variability. *Geophysical Research Letters* **27**: 3353–3356.

Taylor RG, Todd M, Kongola L, Nahozya E, Maurice L, Sanga H, MacDonald A. 2013. Evidence of the dependence of groundwater resources on extreme rainfall in East Africa. *Nature Climate Change* **3**: 374–378.

Tashie AM, Mirus BB, Pavelsky TM. 2015. Identifying long-term empirical relationships between storm characteristics and episodic groundwater recharge. *Water Resources Research* **52**. DOI:10.1002/2015WR017876.

Trambauer P, Dutra E, Maskey S, Werner M, Pappenberger F, van Beek LPH, Uhlenbrook S. 2014. Comparison of different evaporation estimates over the African continent. *Hydrology and Earth System Sciences* **18**: 193–212.

van Beek LPH, Wada Y, Bierkens MFP. 2011. Global monthly water stress: I. Water balance and water availability. *Water Resources Research* **47**: W07517. DOI:10.1029/2010WR009791.

Vicente-Serrano SM, Beguería S, López-Moreno JI. 2010. A multi-scalar drought index sensitive to global warming: the standardized precipitation evapotranspiration index—SPEI. *Journal of Climate*. DOI:10.1175/2009JCLI2909.

Vivoni ER, Aragón CA, Malczynski L, Tidwell VC. 2009. Semiarid watershed response in central New Mexico and its sensitivity to climate variability and change. *Hydrology and Earth System Sciences* **13**: 715–733. DOI:10.5194/hess-13-715-2009.

Wada Y, van Beek LPH, Bierkens MFP. 2011. Modelling global water stress of the recent past: on the relative importance of trends in water demand and climate variability. *Hydrology and Earth System Sciences* **15**. DOI:10.5194/hess-15-3785-2011.

Wada Y, van Beek LPH, van Kempen CM, Reckman JWTM, Vasak S, Bierkens MFP. 2010. Global depletion of groundwater resources. *Geophysical Research Letters* **37**: L20402. DOI:10.1029/2010GL044571.

Wada Y, van Beek LPH, Sperna Weiland FC, Chao BF, Wu Y-H, Bierkens MFP. 2012. Past and future contribution of global groundwater depletion to sea-level rise. *Geophysical Research Letters* **39**: L09402. DOI:10.1029/2012GL051230.

Wada Y, Wisser D, Bierkens MFP. 2014. Global modeling of withdrawal, allocation and consumptive use of surface water and groundwater resources. *Earth System Dynamics* **5**: 15–40. DOI:10.5194/esd-5-15-2014.

Wada Y, Bierkens MFP. 2014. Sustainability of global water use: past reconstruction and future projections. *Environmental Research Letters* **9**, 104003. DOI:10.1088/1748-9326/9/10/104003.

Wang L, Dochartaigh BO, MacDonald AM. 2010. A literature review of recharge estimation and groundwater resource assessment in Africa. British Geological Survey Internal Report, IR/10/051, 31 pp.

